



## Two decades of spatiotemporal variations in subduction zone coupling offshore Japan

John P. Loveless <sup>a,\*</sup>, Brendan J. Meade <sup>b</sup>

<sup>a</sup> Department of Geosciences, Smith College, 44 College Lane, Northampton, MA 01063, USA

<sup>b</sup> Department of Earth and Planetary Sciences, Harvard University, 20 Oxford Street, Cambridge, MA 02138, USA

### ARTICLE INFO

#### Article history:

Received 21 July 2015

Received in revised form 21 December 2015

Accepted 22 December 2015

Available online xxxx

Editor: P. Shearer

#### Keywords:

subduction zone

Japan

coupling

earthquake cycle

### ABSTRACT

Spatial patterns of interplate coupling on global subduction zones can be used to guide seismic hazard assessment, but estimates of coupling are often constrained using a limited temporal range of geodetic data. Here we analyze ~19 years of geodetic observations from the GEONET network to assess time-dependent variations in the spatial distribution of coupling on the subduction zones offshore Japan. We divide the position time series into five, ~3.75-year epochs each decomposed into best-fit velocity, annual periodic signals, coseismic offsets, and postseismic effects following seven major earthquakes. Nominally interseismic velocities are interpreted in terms of a combination of tectonic block motions and earthquake cycle activity. The duration of the inferred postseismic activity covaries with the linear velocity. To address this trade-off, we assume that the nominally interseismic velocity at each station varies minimally from epoch to epoch. This approach is distinct from prior time-series analysis across the earthquake cycle in that position data are not detrended using preseismic velocity, which inherently assumes that interseismic processes are spatially stable through time, but rather the best-fit velocity at each station may vary between epochs. These velocities reveal significant consistency since 1996 in the spatial distribution of coupling on the Nankai subduction zone, with variation limited primarily to the Tokai and Bungo Channel regions, where long-term slow slip events have occurred, and persistently coupled regions coincident with areas that slipped during historic great earthquakes. On the Sagami subduction zone south of Tokyo, we also estimate relatively stable coupling through time. On the Japan-Kuril Trench, we image significant coupling variations owing to effects of the 1994  $M_w = 7.7$  Sanriku-oki, 2003  $M_w = 8.2$  Tokachi-oki, and 2011  $M_w = 9.0$  Tohoku-oki earthquakes. In particular, strong coupling becomes more spatially extensive following the 1994 event until 2011, coseismic-sense slip precedes the Tohoku-oki event, and coupling offshore northern Honshu is reduced after the 2011 earthquake. Despite the occurrence of the 2003 Tokachi-oki earthquake, persistent coupling offshore Hokkaido suggests ongoing seismic hazard, possibly similar to past  $M_w \sim 9$ -class earthquakes interpreted from coastal paleoseismic records. This time-dependent analysis of interseismic deformation illuminates rich diversity in the distribution of subduction zone coupling, including spatiotemporal stability in coupling, effective reduction in strongly coupled regions due to aseismic thrust-sense slip events, and broad changes in the distribution of coupling following major earthquakes.

© 2016 Elsevier B.V. All rights reserved.

### 1. Introduction

Over the past two decades, the proliferation of high-precision geodetic observations and occurrence of large earthquakes have enabled imaging of processes spanning the earthquake cycle, including interseismic strain accumulation, abrupt coseismic strain

release, and transient behavior such as postseismic afterslip, post-seismic viscoelastic relaxation of the lower crust and/or upper mantle, and aseismic slip during the nominally interseismic period. Geodetic displacement time series have led to the discovery of spatial variations in interseismic coupling (McCaffrey et al., 2000; Nishimura et al., 2004), constraints on the viscosity of Earth's lower crust (Hearn et al., 2009; Pollitz et al., 2000), and the occurrence of aseismic slow slip events (Dragert et al., 2001; Hirose et al., 1999).

The GEONET GNSS array has measured surface displacement across the Japanese Islands at >800 stations since 1996. These

\* Corresponding author. Tel.: +1 413 585 2657.

E-mail addresses: [jloveless@smith.edu](mailto:jloveless@smith.edu) (J.P. Loveless), [meade@fas.harvard.edu](mailto:meade@fas.harvard.edu) (B.J. Meade).

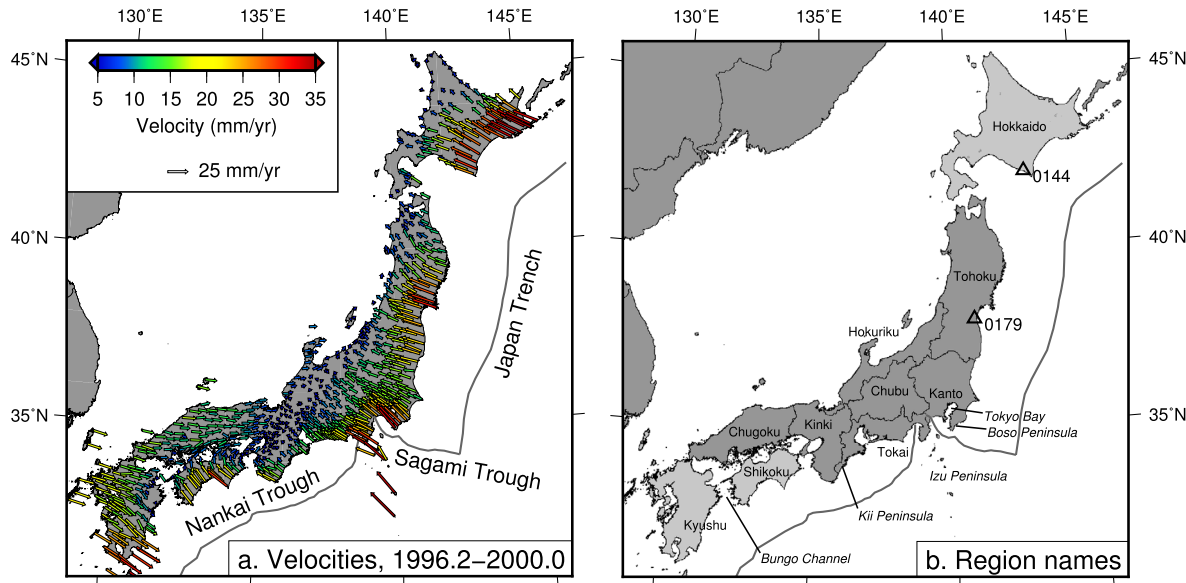


**Fig. 1.** a) Nominally interseismic velocity field for GEONET stations, April 1, 1996–December 31, 1999, expressed relative to the stable Eurasia reference frame of Apel et al. (2006). b) Regions and localities of Japan referred to in the text. The labeled darker gray regions comprise the island of Honshu. Position time series for stations 0144 and 0179 are shown in Fig. 2.

crustal deformation observations have been interpreted as reflecting earthquake cycle processes on the network of crustal faults throughout Japan and the three subduction interfaces offshore (Nankai Trough, Sagami Trough, Japan-Kurile Trench; Fig. 1a) (Hashimoto et al., 2000; Loveless and Meade, 2010; Nishimura et al., 2004). Previous studies have focused on either spatiotemporal evolution of subduction zone coupling on an isolated subduction zone section (Hashimoto et al., 2009; Liu et al., 2010; Mavrommatis et al., 2014; Nishimura et al., 2004), or nationwide tectonics using a limited time period of GEONET observations (Hashimoto et al., 2000; Loveless and Meade, 2010).

Here we analyze GEONET data in five,  $\sim 3.75$ -year epochs spanning April 1996 through December 2014. For each epoch, we fit each station time series with a combination of linear, periodic, step, and exponential functions, which we interpret to represent nominally interseismic deformation related to earthquake cycle processes on the subduction zones and crustal faults, seasonal effects, offsets due to earthquakes and equipment maintenance, and postseismic deformation following large earthquakes, respectively. We use the linear velocity fields as constraints on quasi-static elastic block models, which provide a means for interpreting geodetic observations resulting from the combined effects of tectonic block rotations, earthquake cycle processes (Meade and Loveless, 2009), and volume changes of magma bodies. We use these models to image patterns of subduction zone coupling in each of the five epochs, identifying persistently coupled regions, effects of large earthquakes on subduction zone coupling, and the occurrence of aseismic slip events.

## 2. Methods

### 2.1. Decomposition of displacement time series

We analyze F3 daily coordinates from the Geospatial Information Authority of Japan during five time periods: April 1, 1996–December 31, 1999 (1996.25–2000.00; 3.75 year duration); January 1, 2000–September 24, 2003 (before the  $M_w = 8.2$  Tokachi-oki earthquake offshore Hokkaido, 2000.00–2003.73; 3.73 years); September 25, 2003–June 30, 2007 (2003.73–2007.50; 3.77 years); July 1, 2007–March 10, 2011 (before the  $M_w = 9.0$  Tohoku-oki earthquake offshore northern Honshu, 2007.50–2011.19;

3.69 years); and March 11, 2011–December 31, 2014 (2011.19–2015.00; 3.81 years). For the entire time series, we fit individual station position time series,  $\mathbf{x}(t)$ , where the vector  $\mathbf{x}$  represents the position in the east or north direction, using piecewise linear, periodic, step and exponential functions:

$$\begin{aligned} \mathbf{x}(t) = & \sum_{i=1}^{N_{\text{epoch}}} \mathbf{A}_i * I(t - t_i) + \sum_{j=1}^2 \left( \mathbf{B}_j \sin \frac{2\pi jt}{T_{\text{yr}}} + \mathbf{C}_j \cos \frac{2\pi jt}{T_{\text{yr}}} \right) \\ & + \sum_{k=1}^{N_{\text{step}}} \mathbf{D}_k H(t - t_k) \\ & + \sum_{m=1}^2 \sum_{n=1}^{N_{\text{eq}}} \mathbf{E}_{(2(n-1)+m)} H(t - t_n) \left( 1 - e^{(t_n - t)/\tau_m} \right), \end{aligned} \quad (1a)$$

where

$$I = \begin{cases} 1 & \text{for } t_i \leq t < t_{i+1} \\ 0 & \text{for } t < t_i \text{ and } t \geq t_{i+1} \end{cases}, \quad (1b)$$

and

$$\tau_m = \frac{P_m * T_{\text{yr}}}{-\ln(0.05)}. \quad (1c)$$

$\mathbf{A}$  is the linear slope during each epoch, which we take to reflect the nominally interseismic velocity;  $I$  is an index function defined such that  $I = 1$  for time values within the epoch and zero for times before and after;  $\mathbf{B}$  and  $\mathbf{C}$  are amplitudes of annual and semianual periodic terms;  $\mathbf{D}$  gives the amplitude of steps in the time series corresponding to earthquakes, equipment (antenna) changes, and ordinate-intercepts accompanying linear terms;  $H$  is the Heaviside step function; and  $\mathbf{E}$  is the amplitude of postseismic deformation following specified earthquakes. The decay constants,  $\tau_m$ , correspond to durations  $P_m$  (in years) following an earthquake when the exponential function reaches 95% peak asymptotic amplitude  $\mathbf{E}$ . In all terms,  $t$  is the time in days since the beginning of the analysis time period,  $T_{\text{yr}}$  is the duration of a year in days, and subscripted  $t$  values in linear, step, and exponential functions refer to dates of epoch initiation, offsets, and major earthquakes, respectively. We consider 23 values of  $\tau_2$ , corresponding to durations of exponential signal ranging from 6 months to 10 years

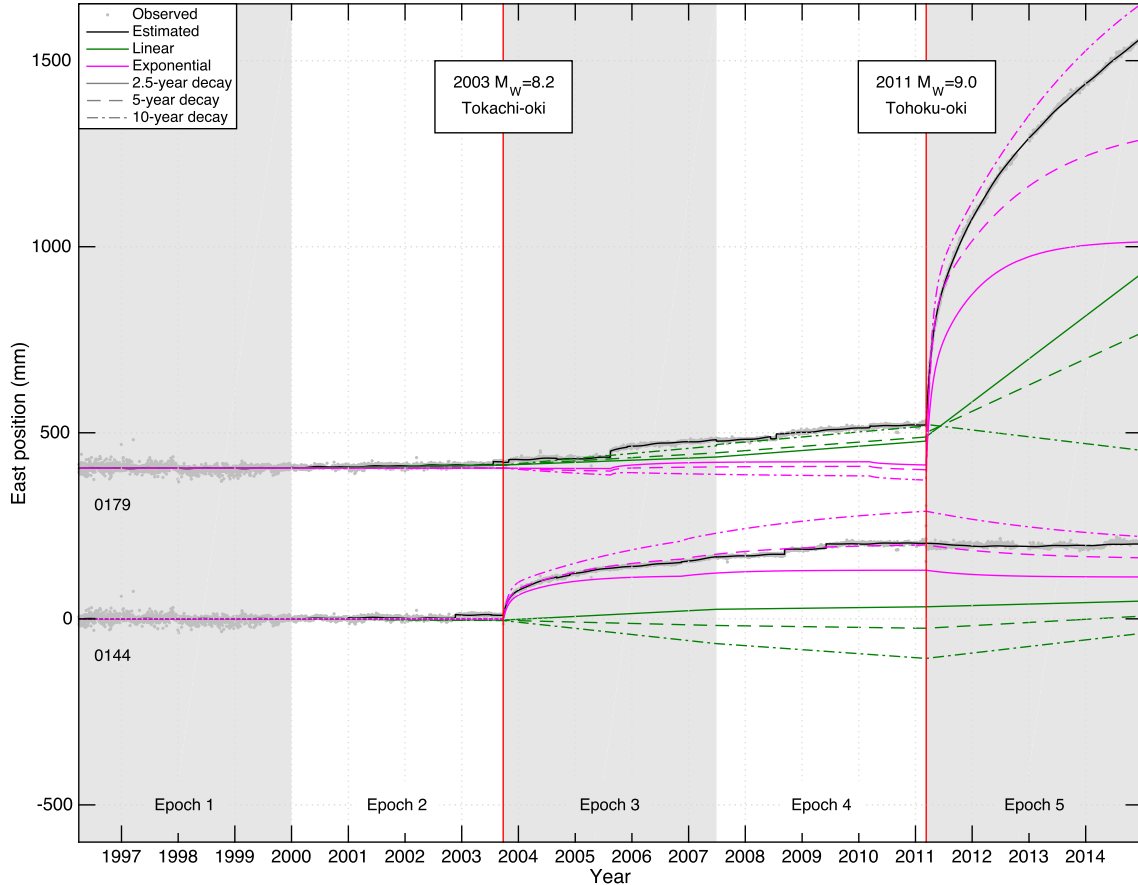


**Fig. 2.** East component of the observed position time series (gray dots) at stations on the Pacific coast of Hokkaido (0144) and Tohoku (0179) with fits estimated using Equation (1) (black line). Contributions to the fit from the piecewise linear (green) and exponential (magenta) terms are each shown for three assumed exponential decay durations: 2.5, 5, and 10 years as solid, dashed, and dash-dot lines, respectively. Red lines show timing of the 2003 Tokachi-oki and 2011 Tohoku-oki earthquakes. Observed, estimated, and linear plots have been detrended using the Epoch 1 (April 1, 1996–December 31, 1999) linear velocity estimate so that deviation from horizontal shows each epoch's relative change in velocity (e.g., Fig. 5). Station locations are shown in Fig. 1. (For interpretation of the references to color in this figure legend, the reader is referred to the web version of this article.)

in 6 month intervals, plus 25, 50, and 100 years. In all trials, we also fit a function described by  $\tau_1$  with a 3-month decay, capturing rapid evolution of surface deformation near the earthquake source. However, in cases where the sign of  $\mathbf{E}$  corresponding to a  $\tau_1$  term differs from that of the associated  $\tau_2$  term, we eliminate the  $\tau_1$  term and estimate  $\mathbf{E}$  for the longer duration only.

For all epochs, we evaluate the quality of fit to the data as the mean magnitude of daily position residuals between observations and total fit from Equation (1). This approach differs from formal calculation of uncertainties from the model covariance matrix, which is not straightforward given the absence of reported uncertainties on F3 position data. The mean residuals serve as relative weights on linear velocities in our inversion for earthquake cycle processes. Epoch-averaged mean residual positions range from 1.57 mm (north component of Epoch 4) to 5.55 mm (east component of Epoch 1).

We estimate coseismic jumps for up to 200 earthquakes (1996–2014,  $M_w \geq 6$ , depth  $\leq 50$  km as given in the Global CMT catalog) and consider postseismic deformation following the 2003  $M_w = 8.2$  Tokachi-oki, 2004  $M_w = 7.2$ –7.3 off-Kii Peninsula, 2005  $M_w = 7.2$  Miyagi, 2006  $M_w = 8.3$  Kuril Islands, 2008  $M_w = 6.9$  Iwate-Miyagi Nairiku, 2010  $M_w = 6.5$  Fukushima, and 2011  $M_w = 9.0$  Tohoku-oki events. We follow an approach similar to that of Ikuta et al. (2012), estimating coseismic steps and exponential postseismic terms at stations within  $10^{0.36M_w - 0.15}$  km of the earthquake epicenter. For the Tokachi-oki and Tohoku-oki earthquakes, we estimate postseismic deformation at all stations.

The scaling of the magnitude-dependent distances was evaluated by eye, assessing whether or not displacement time series exhibited clear coseismic offsets and therefore likely include postseismic deformation.

## 2.2. Interpretation of time series terms

The exponential term in Equation (1a) corresponding to values of assumed  $\tau_2$  negatively covaries with velocity  $\mathbf{A}$ , with the longest decay durations producing exponential signals inversely proportional to the estimated linear term (Figs. 2, 3). In some cases of long  $\tau_2$ , the exponential contribution to the functional fit to the position time series shows a different sign than the linear term. For large Pacific Coast earthquakes, which produce eastward (trenchward) co- and postseismic displacements, such fitting of the position data could be interpreted as large magnitude viscoelastic relaxation and/or afterslip, producing eastward movement, slowed by westward motion from resumed interseismic coupling, yielding a net slow eastward signal (e.g., the 10-year fit in Fig. 2).

Covariance between exponential and linear terms for epochs following large earthquakes (Fig. 3) leads to, particularly in the case of long assumed decay times, degeneracy in uniquely mapping time series analysis terms to either postseismic viscoelastic relaxation or megathrust slip behavior. In this analysis, we make the end-member assumption that exponential terms represent time-decaying postseismic deformation, comprising combined megathrust afterslip and viscoelastic relaxation, with decay times

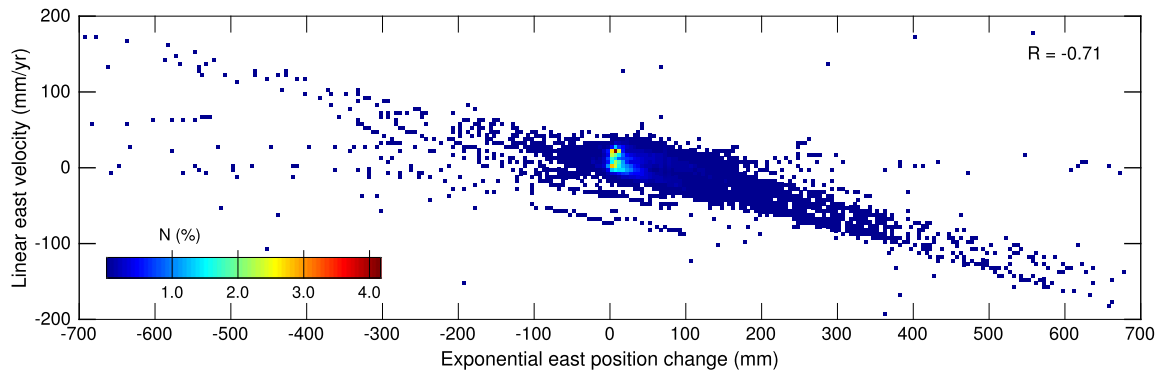


**Fig. 3.** Covariance between estimated linear velocity (**A** term of Equation (1)) and exponential position change (**E** term of Equation (1)) in the east direction during Epoch 3 (following the Tokachi-oki earthquake), evaluated for all stations across the suite of trial exponential decay durations we test in our time series analysis. The color scale indicates the normalized frequency distribution of exponential-linear combinations. (For interpretation of the references to color in this figure legend, the reader is referred to the web version of this article.)

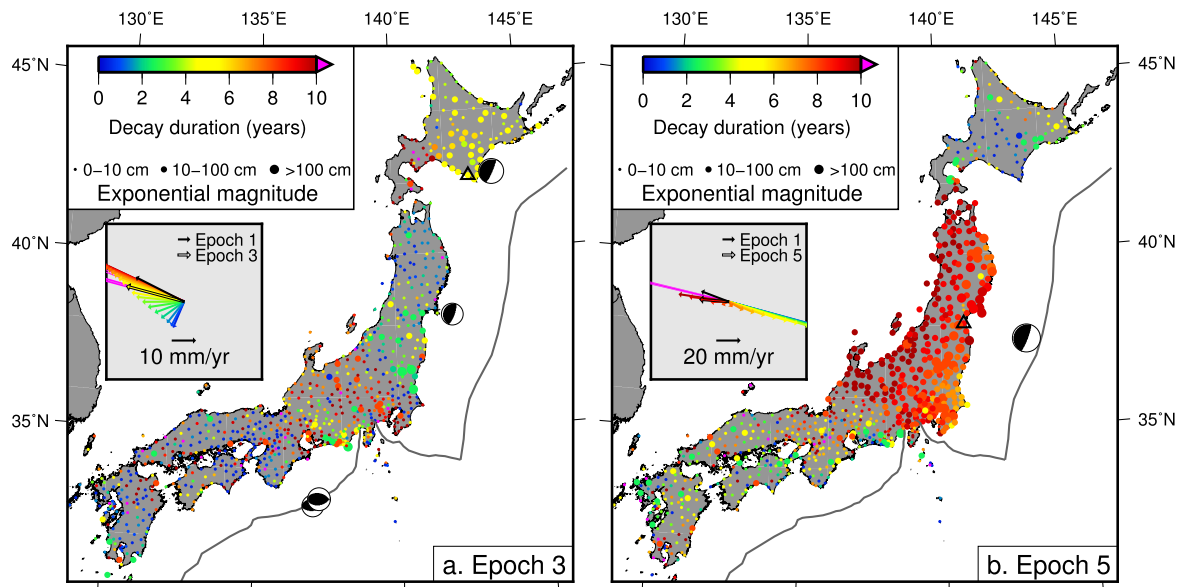


**Fig. 4.** Estimated postseismic duration at each station in the epoch following the a) 2003 Tokachi-oki and b) 2011 Tohoku-oki earthquakes, the Global CMT focal mechanism for each of which is shown. We estimate the postseismic duration by assuming that, for these post-earthquake epochs, a linear contribution to the fit to the position time series (i.e., velocity) varies little compared to the velocity estimated for Epoch 1 (1996.3–2000.0). We do so by choosing the variable that controls the decay duration of an exponential function we use to model postseismic position change. Symbol size indicates the total estimated displacement of the exponential function from the time of the earthquake through the end of the noted epoch. The inset of each panel shows the epoch's linear fit (velocity) vectors at a single station (location indicated by a black triangle) given the tested range of postseismic decay durations. The Epoch 1 velocity vector is shown as a solid black vector, and the chosen candidate vector for each postseismic epoch is outlined in black. (For interpretation of the references to color in this figure legend, the reader is referred to the web version of this article.)

specified by  $\tau_m$  values. The linear term is interpreted to represent convolved contributions from coupling on megathrusts, rotation of crustal blocks, and elastic strain accumulation due to locking on block boundaries. In other words, estimated linear terms for each epoch represent the velocity field we use to constrain quasi-static elastic block models of interseismic deformation. This velocity decomposition may map some viscoelastic relaxation onto megathrust and microplate slip and/or slip deficit. Though afterslip and resumption of interseismic coupling are spatiotemporally varying processes, we here consider estimated deformation patterns as reflecting time-averaged earthquake cycle behavior throughout each epoch.

### 2.3. Constructing minimally variable velocity fields

As a basis for evaluating temporal stability of spatial patterns of subduction zone coupling, we determine interseismic velocities that vary minimally from epoch to epoch. Due to infrequent macroscale seismicity from 1996–2000 (Loveless and Meade, 2010;

Sagiya et al., 2000), we use the Epoch 1 velocity field (Fig. 1) as a reference epoch against which subsequent epoch velocities are compared. To construct what we term minimally variable velocity fields (MVVF), we choose, at each station  $s$ , during each epoch  $\varepsilon$ , the  $\tau_2$  value that yields a velocity vector,  $\mathbf{A}$ , most similar in magnitude to that estimated using a 1-year decay duration during Epoch 1,

$$\hat{\tau}_2(s, \varepsilon) = \arg \min_{\tau_2} (\|\mathbf{A}(s, \varepsilon, \tau_2) - \mathbf{A}(s, 1, 1)\|). \quad (2)$$

In other words, we select the duration of postseismic deformation at each station assuming that subduction zone coupling varies as little as possible through time (Fig. 4).

Construction of the MVVF is consistent with the formal assumption of prior geodetic imaging studies spanning multiple earthquake cycles (Ergintav et al., 2009) in that the linear contribution to the time series fit, interpreted to represent interseismic strain accumulation, is similar through time at each station. However, the MVVF is distinct in that a station's interseismic velocity

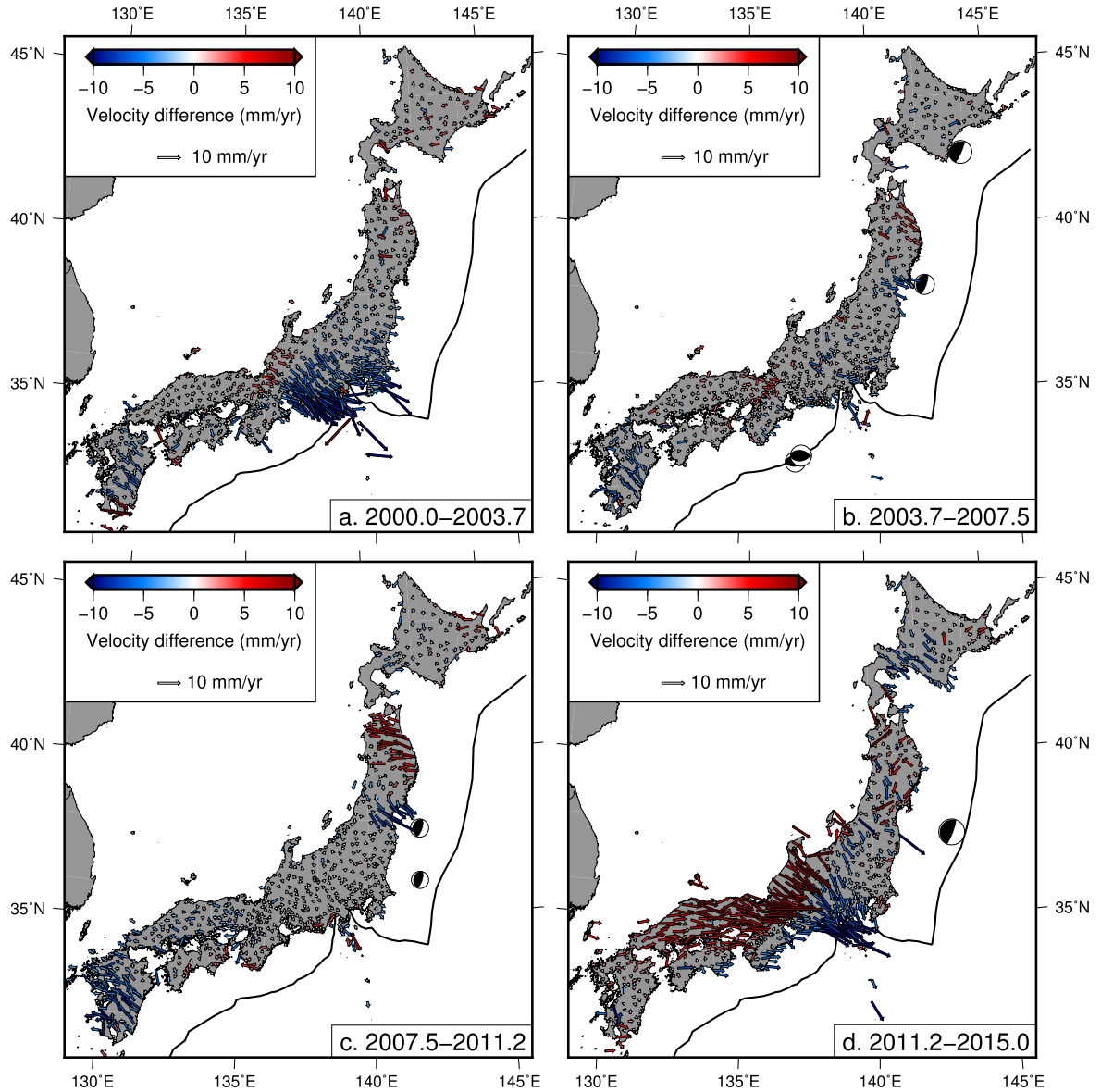


**Fig. 5.** Changes in nominally interseismic velocities through time, relative to Epoch 1 (1996–1999). Vector color indicates an increase (red) or decrease (blue) in speed, length indicates the absolute value of speed change, and direction shows the direction change. For example, the blue vectors in (a) indicate that stations in the Tokai region moved up to 18 mm/yr more slowly and more southeasterly during Epoch 2 (2000.0–2003.7) than during Epoch 1. (For interpretation of the references to color in this figure legend, the reader is referred to the web version of this article.)

can and does vary through time (Figs. 4, 5), as the station velocity is not formally constrained to remain temporally constant but rather is as similar as possible to the Epoch 1 velocity. This assumption may underestimate true variation in interseismic coupling and overestimate postseismic deformation, points we return to in Sections 4.1 and 4.2.

#### 2.4. Block modeling

We filter from each epoch velocity field poorly constrained and spatially inconsistent stations, removing those with mean residual positions  $\geq 12.5$  mm and those that differ from the average velocity at neighboring stations within 20 km by  $\geq 5$  mm/yr. We then place each velocity field into the reference frame of Apel et al. (2006), using a 6-parameter (rotation plus translation) transformation to align velocities at stations collocated in GEONET fields and the Apel et al. (2006) field. The transformation parameters are estimated by linear least-squares fitting that aligns the Epoch 1 velocity field with that of Apel et al. (2006). To facilitate comparison

of model results, we retain only those stations that are present in all epochs.

Using a three-dimensional elastic block modeling framework (Meade and Loveless, 2009), we simultaneously estimate Euler poles for 20 tectonic blocks; spatially variable slip deficit rates on the Japan–Kuril Trench, Nankai Trough, and Sagami Trough subduction zones; and magma chamber volume change rates at 3 locations. The block geometry is as given in Loveless and Meade (2010), based on plate boundary models (Bird, 2003), the digital active fault map of Japan (Nakata and Imaizumi, 2002), and previous crustal deformation studies (Hashimoto and Jackson, 1993; Nakamura, 2004; Nishimura and Hashimoto, 2006; Nishimura et al., 2007). The subduction zone interfaces are tessellated using triangular dislocation elements (TDEs), with the interface geometry defined by various geophysical studies (Furuse and Kono, 2003; Hirose et al., 2008; Toda et al., 2008). We use each realization of the velocity field, described above, along with *a priori* assumptions that the subduction zone slip deficit rate distribution be a) spatially smooth across the plate interface, with the strength of this

constraint set so that the maximum magnitude of slip deficit is similar to the relative plate motion projected onto the subduction zone elements (Loveless and Meade, 2010); b) zero on TDEs at the deep extent of each subduction zone, representing a transition to fault creep behavior; and c) zero on TDEs lining the subduction trenches. We also show results for models in which this latter constraint is relaxed, reflecting poor resolution of coupling patterns near the subduction trench (Loveless and Meade, 2011) and the possibility that interseismic coupling may extend to the trench (Gagnon et al., 2005). We also estimate volume change rates by representing magma bodies as buried spherical sources, relating radial surface velocities around each body due to unit volume change (Mogi, 1958).

### 3. Results

#### 3.1. Estimated duration of postseismic effects

As an illustration of MVVF construction, we show stations symbolized by the postseismic decay duration that yields temporal consistency in linear velocity A for Epochs 3 and 5, corresponding to the time periods following the Tokachi-oki and Tohoku-oki earthquakes, respectively (Fig. 4). In general, longer decay durations are required at stations around the earthquake source regions. Notable exceptions include long (7–10-year) decay times around Tokai during Epoch 3, which may reflect a long-term slow slip event from 2000–2005 beneath Tokai (Miyazaki et al., 2006; Ochi and Kato, 2013), and longer decay times estimated on the west coast of northern Honshu (10 years) than on the east coast (8 years) following the Tohoku-oki earthquake. The chosen decay constants for Epochs 3 and 5 can be interpreted as the duration of postseismic deformation following the Tokachi-oki and Tohoku-oki earthquakes, respectively, under the MVVF assumption that the spatial pattern of interseismic deformation changes little through time. Short-wavelength fluctuations in postseismic duration may reflect localized temporal variation in earthquake cycle processes distinct from great earthquakes, including smaller subduction and crustal earthquakes, transient deformation, and volcano-related deformation (Table S6).

#### 3.2. Interseismic velocities through time

We examine changes in MVVF vectors through time relative to Epoch 1 (Fig. 1a). In the following discussion, references to regions (Fig. 1b) are, in general, to their Pacific coastal sections, and references to speed and direction are relative to those of Epoch 1, with numerical values indicating maximum speed difference.

During Epoch 2 (Fig. 5a), the most discernable velocity change is slower (by up to ~18 mm/yr), more trenchward (southeast) motion in Tokai and Kanto. Additional velocity changes include slower (7 mm/yr), more landward (northwest) motion of the majority of Kyushu; faster (6 mm/yr) and more eastward motion in southern Hokuriku; slightly slower (5 mm/yr), more trenchward motion in southern Tohoku (38°N); and faster (5 mm/yr), more landward motion in northern Tohoku.

During Epoch 3 (Fig. 5b), velocity change in Hokkaido, with the exception of a few scattered stations, is small, suggesting little change in interseismic deformation following the 2003 Tokachi-oki earthquake. Northern Tohoku again shows faster (8 mm/yr), more landward velocities, while central Tohoku shows continued slower (8 mm/yr), trenchward motion. The Kanto-Tokai region shows little velocity change; a cluster of slower (8 mm/yr), southeast vectors appears on the Izu Peninsula, which may reflect offshore volcanic deformation. Hokuriku and Kyushu show velocity changes similar to those of Epoch 2, indicating little change in motion between Epochs 2 and 3.

Comparing Epoch 4 (Fig. 5c) to Epoch 1, slowed (10 mm/yr), northwestward velocities again characterize much of Kyushu, indicating consistency in velocity since 2000.0. This pattern is also present in Chugoku, with velocities decreased by up to 6 mm/yr. Velocity changes in Tohoku (faster (9 mm/yr) and more landward in the north, slower (12 mm/yr) and more trenchward in the south) are accentuated since Epoch 3, showing a pattern of counterclockwise rotation. Velocities in southwest Hokkaido are slower (4 mm/yr) and more northeasterly, but stations in the northeast move faster (5 mm/yr) and more landward.

Velocity changes in Epoch 5 (Fig. 5d) are randomly oriented across much of northern Honshu, near the source region of the 2011 Tohoku-oki earthquake, with more spatially coherent patterns in other regions. In southern Hokkaido, velocities are slower (10 mm/yr) and more southeasterly than in Epoch 1. In the coastal Tokai-southern Kanto region, velocities are trenchward and slowed (20 mm/yr) compared to those of Epoch 1, showing a pattern similar to that of Epoch 2. To the northwest, in northern Chubu and western Hokuriku, stations show similar directional change but move faster (26 mm/yr) than during Epoch 1, suggesting shortening in Chubu. The spatial coherence and large magnitude of these velocity changes suggest that far-field postseismic deformation may be inadequately modeled, and changes in interseismic coupling inferred from these velocities may in fact convolve post- and interseismic processes. In western Kinki and Chugoku, vectors are mostly faster (13 mm/yr) and more eastward, reversing the pattern of Epoch 4. Much of Kyushu shows little velocity change relative to Epoch 1, though faster (7 mm/yr), eastward vectors characterize the southern extreme.

#### 3.3. Spatiotemporal variation in subduction zone coupling

Using MVVF velocity estimates for each epoch as constraints on block models, we simultaneously estimate tectonic plate motions and spatially variable slip deficit rates on subduction zone interfaces. These rates are converted to coupling coefficients by normalizing the slip deficit rate by the relative block motion rate projected onto each triangular element. We place no bounds on the estimated slip deficit rate, instead choosing smoothing values that result in rates on no more than 10% of elements of each subduction zone exceeding the plate convergence rate. Given the spatial complexity in estimated coupling distributions, we focus our discussion on regions we estimate to be strongly coupled (slip deficit rate  $\geq 80\%$  relative block motion rate, Fig. 6) and regions that experience thrust-sense slip (at  $\geq 10\%$  the block motion rate, Fig. 7), which we interpret as aseismic creep occurring during the nominally interseismic period. We estimate uncertainties in coupling as the standard deviation about the mean from Monte Carlo simulations, inverting 5000 realizations of the velocity field predicted by forward modeling of the slip deficit distribution, perturbed by noise proportional to the station uncertainties. The along-strike extent of strongly coupled regions is generally consistent between models in which slip deficit along the subduction trenches is constrained to be zero, which we refer to as trench-creeping (TC) models (Fig. 6), and those in which this constraint is not applied (trench-unconstrained (TU) models). The near-trench behavior of many subduction megathrusts is poorly constrained by land-based geodetic data due to great ( $\geq 200$  km) distance between stations and the trench (Loveless and Meade, 2011). Though coseismic slip during the Tokoku-oki earthquake reached the trench, dynamic overshoot (Ide et al., 2011) is a hypothesis that may explain observed shallow rupture, even in the absence of persistent shallow coupling. We present the TC models, in which smoothing features from poorly resolved regions do not propagate down-dip where resolution is greater, but we discuss comparisons with TU models

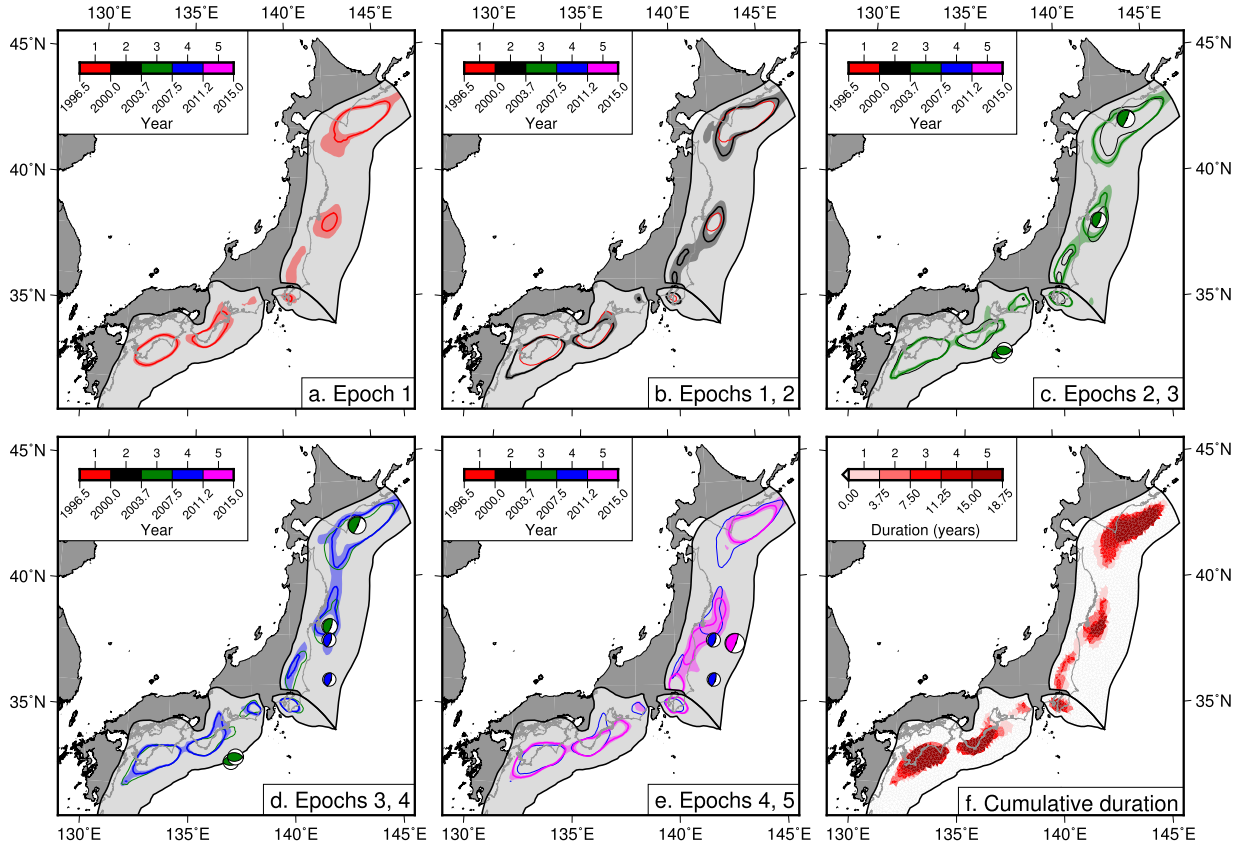


**Fig. 6.** Spatiotemporal evolution of strong coupling on the Japanese subduction zones. We use the nominally interseismic, minimally variable velocity fields to estimate the spatial distribution of subduction zone coupling for each epoch. a–e) Colored contour lines show regions where estimated slip deficit rate is  $\geq 80\%$  the relative tectonic block motion rate (i.e.,  $\geq 80\%$  coupled) during the listed epochs (current: thick; prior: thin). These contours represent the mean coupling distribution from inversion of 5000 realizations of the velocity field, with synthetic noise proportional to station uncertainty. Translucent shaded regions represent the standard deviation about the mean of strong coupling estimated for the current epoch. For example, the thick black contours in (b) show strongly coupled regions during Epoch 2, and the thin red contours show strong coupling during Epoch 1 (repeated from panel a). The shaded gray regions surrounding the black contour indicate the minimum and maximum areas of  $\geq 80\%$  coupling during Epoch 2 from the uncertainty estimation, reflecting the mean coupling (black contour) plus and minus, respectively, the standard deviation. Focal mechanisms show earthquakes that occurred during each epoch, with the color of the compressive quadrant indicating the timing. f) Duration of strong coupling. The color of each subduction zone element reflects the summed number of  $\sim 3.75$ -year epochs in which we estimate strong coupling, using the mean values from our Monte Carlo simulations. (For interpretation of the references to color in this figure legend, the reader is referred to the web version of this article.)

and show equivalent TU results in Figs. S1–S3, corresponding to TC results in Figs. 6–8.

We find  $\geq 80\%$  coupling during Epoch 1 offshore Hokkaido and central Tohoku ( $38^\circ\text{N}$ ) on the Japan Trench; on the western Sagami Trough; and beneath eastern Tokai, and in 2 regions on the Nankai Trough beneath Shikoku and the Kii Peninsula-Tokai region (Fig. 6a). During Epoch 2 (Fig. 6b), coupling is similar to that of Epoch 1 in both TC and TU models, though with southwest expansion of the Shikoku patch to offshore central Kyushu, representing an area increase of nearly 50%.

In Epoch 3 (Fig. 6c), following the 2003 Tokachi-oki earthquake, coupling migrates deeper than in prior epochs at the bend in the Japan-Kuril Trench at  $42^\circ\text{N}$ , to  $\sim 60$  km compared to  $\sim 40$  km. Offshore eastern Hokkaido, the depth extent of coupling is less than in prior epochs (reduced from  $\sim 60$  km to  $\sim 40$  km), and instead we estimate a region of deep, thrust-sense slip (Fig. 7c). Offshore Tohoku, we estimate a deeper region of strong coupling. The TC model also extends to the north by about  $1^\circ$ , representing an increase in area of strong coupling of 25%, and the TU model shifts deeper than in Epoch 2, leaving the trench less coupled (Fig. S1c). On the Sagami Trough, the extent of strong coupling appears similar as during Epochs 1 and 2. On the Nankai Trough, strong coupling appears similar to that of Epoch 2 but with an additional patch of coupling near the northeast extent.

During Epoch 4 (Fig. 6d), prior to the 2011 Tohoku-oki earthquake, the down-dip extent of the Tohoku coupling patch is narrower (by about 30 km in the TC model) than during prior epochs near its southern limit, and we estimate forward sense slip on the deep interface from  $35^\circ$ – $37^\circ\text{N}$ . The Sagami Trough shows coupling similar to that of Epochs 1 and 3. On the Nankai subduction zone, coupling near Tokai and the Kii Peninsula is similar to Epoch 3 but the southwest coupling patch contracts to an area similar to that during Epoch 1.

The spatial distribution of coupling on Nankai is consistent through Epoch 5, with a southwestern patch intermediate in its southwest extent to that of Epochs 1 and 4, and Epochs 2 and 3, and shallow coupling through the Tokai region to  $137^\circ\text{E}$  (Fig. 6e). The strongly coupled region on the Sagami Trough shows growth since prior epochs, about 40% larger than in Epoch 4. On the Japan Trench, we estimate strong coupling beneath the coastline between  $36$ – $38^\circ\text{N}$  and offshore  $39^\circ\text{N}$  in TC and TU models. Coupling offshore Hokkaido is substantially reduced in southwest extent, with the patch terminating around the southeast corner of the island; the overall area of this coupled patch is about half that of Epoch 4.

### 3.4. Spatiotemporal variation in aseismic subduction zone slip

Aseismic thrust-sense slip exceeding 10% of local relative block motion rate is concentrated mostly near the downdip extent of

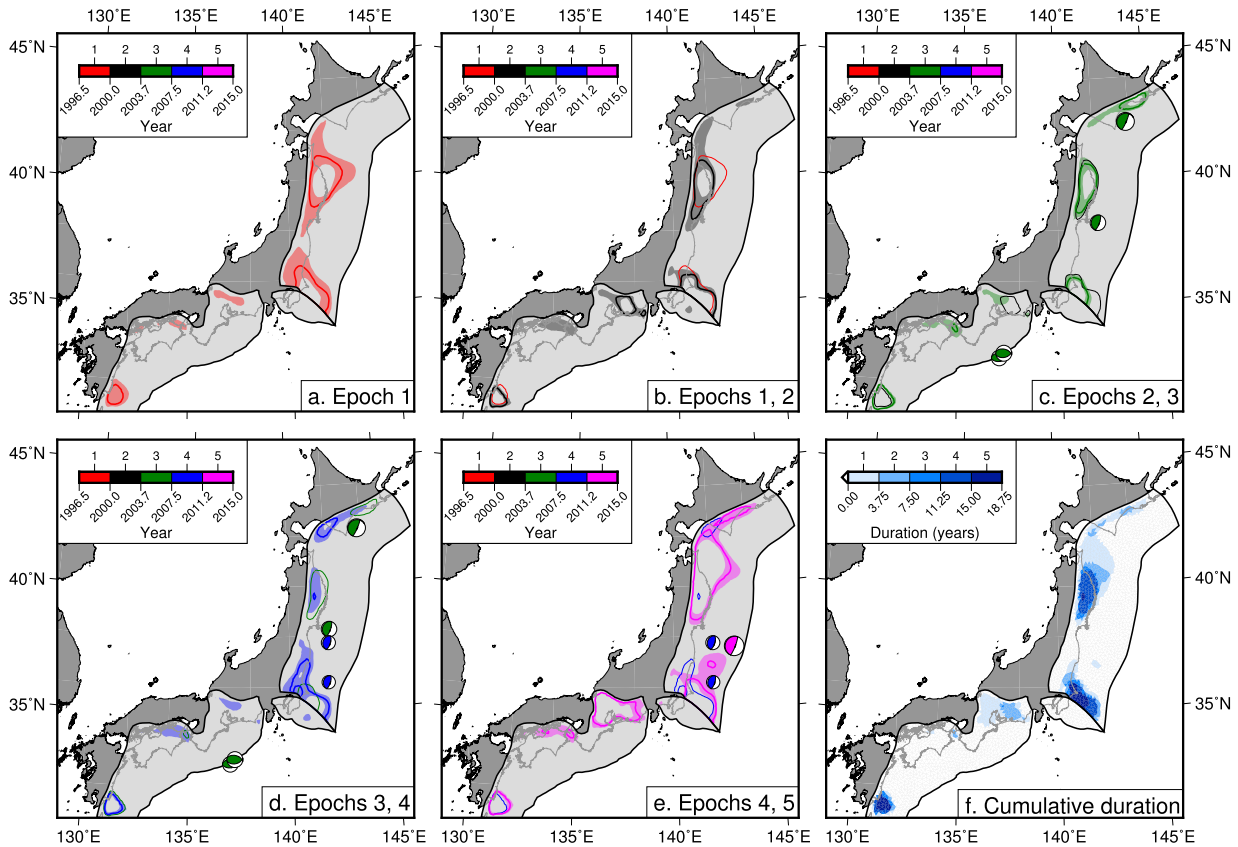


**Fig. 7.** Spatiotemporal evolution of thrust-sense slip on the Japanese subduction zones. As in Fig. 6, we use the nominally interseismic, minimally variable velocity fields to estimate the spatial distribution of subduction zone slip for each epoch and use a Monte Carlo simulation to estimate uncertainties in slip contours. a–e) Hollow contours show regions where estimated thrust-sense slip is  $\geq 10\%$  the magnitude of relative tectonic block motion rate during the listed epochs (current: thick; prior: thin), and the translucent shaded regions show the spatial range of estimated thrust-sense slip the current epoch based on our uncertainty analysis, as described for Fig. 6. Focal mechanisms are as described for Fig. 6. f) Duration of aseismic thrust-sense slip (of rate  $\geq 10\%$  relative plate motion). The color of each subduction zone element reflects the summed number of  $\sim 3.75$ -year epochs in which we estimate aseismic slip, using the mean values from our Monte Carlo simulations as described in Fig. 6. (For interpretation of the references to color in this figure legend, the reader is referred to the web version of this article.)

modeled subduction interfaces. As a result, the distribution of thrust-sense slip is similar between TC and TU models.

During Epoch 1 (Fig. 7a), thrust-sense slip is present on the Nankai subduction interface beneath the southeast coast of Kyushu, and on the Japan Trench subduction zone, we find a  $\sim 200$ -by- $100$  km patch of thrust slip near  $40^{\circ}\text{N}$ , downdip from the source area of the 1994 Sanriku-oki earthquake (Heki et al., 1997). During Epoch 2 (Fig. 7b), notable differences in thrust slip distribution are the presence of a patch around  $137^{\circ}\text{E}$  around Tokai, and  $\sim 30\%$  reduction in area of the Sanriku-oki patch.

During Epoch 3 (Fig. 7c), after the 2003 Tokachi-oki earthquake, we image regions of thrust slip beneath the northern half of the east coast of Hokkaido and beneath northern Tohoku, similar to the Epoch 2 Sanriku-oki patch. The thrust-sense slip patch imaged beneath Tokai in Epoch 2 does not appear during Epoch 3, though a small patch between the Kii Peninsula and Shikoku does.

During Epoch 4, deep slip on the Japan Trench interface spans  $35^{\circ}$ – $37^{\circ}\text{N}$ , with an insignificant patch near  $39^{\circ}\text{N}$ . Beneath the Hokkaido coastline, slip occurs in a region  $\sim 30\%$  smaller and shifted to the southwest  $\sim 100$  km relative to Epoch 2.

In Epoch 5 (Fig. 7e) a broad, deep region of thrust-sense slip on the Japan Trench, from  $38^{\circ}$ – $43^{\circ}\text{N}$ , spans the Japan-Kuril Trench bend off southern Hokkaido. A shallower ( $\leq 40$  km depth) region of aseismic slip also occurs at  $36^{\circ}\text{N}$ . Thrust-sense slip occurs across a broader depth range on the Nankai interface than during previous epochs. In particular, we estimate slip beneath Tokai from 20–50 km depth.

## 4. Discussion

### 4.1. Implications of interseismic–postseismic covariance

A recent focus of research in earthquake science has been on using GPS to distinguish the effects of postseismic afterslip and viscoelastic relaxation following major earthquakes (Diao et al., 2013; Sun et al., 2014; Yamagiwa et al., 2015). Diao et al. (2013), by comparing afterslip models with and without viscoelastic relaxation, suggest that viscoelastic relaxation contributed nominally to the postseismic deformation within the first 1.5 years following the Tohoku-oki earthquake but accounts for an increasing proportion of deformation through time. Yamagiwa et al. (2015), using viscoelastic modeling of offshore and onshore GPS displacements, suggest that trenchward postseismic motion of GEONET stations represents primarily the effect of afterslip, which persists for about 2.5 years following the Tohoku-oki earthquake. On the other hand, Sun et al. (2014) interpret the combination of landward postseismic motion observed at seafloor geodetic sites above the Tohoku-oki rupture area and the trenchward-moving coastal sites as resulting primarily from viscoelastic relaxation.

While these analyses focus on short-term postseismic deformation, longer-term studies must take into account the possibility that the impact of interseismic deformation on geodetic position time series is not necessarily the same as prior to the earthquake. In other words, detrending the entire time series using pre-seismic, nominally secular station velocity (Ergintav et al., 2009) may not be appropriate, since that velocity arises from a particular dis-

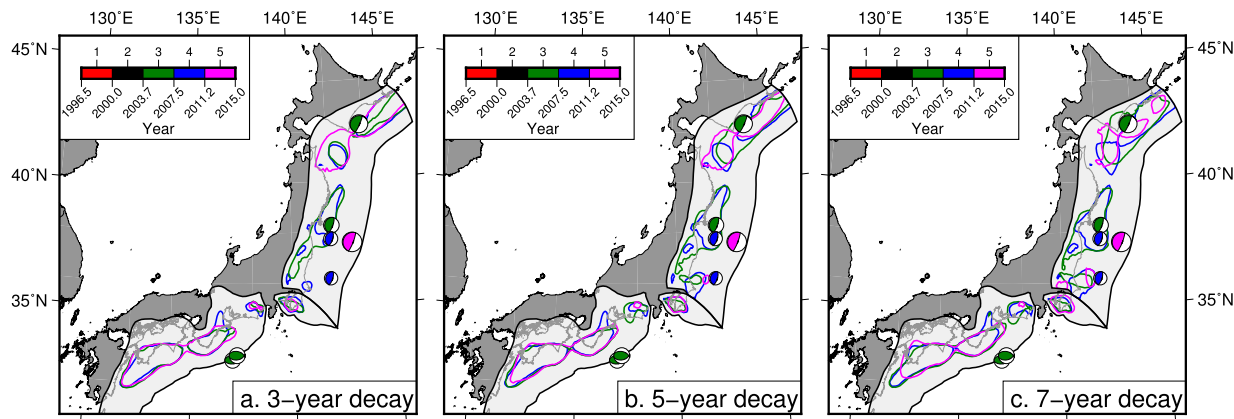


**Fig. 8.** Estimated distribution of strong ( $\geq 80\%$ ) coupling for all epochs assuming a temporally constant postseismic decay function. We show only the estimates for Epochs 3–5; because the first earthquake after which we estimate a postseismic contribution to the GPS time series occurs at the beginning of Epoch 3, the coupling estimated for Epochs 1 and 2 appears similar regardless of assumed decay time. For visual clarity, we do not show uncertainties on the estimated contours. Focal mechanisms are as described in Fig. 6. (For interpretation of the references to color in this figure legend, the reader is referred to the web version of this article.)

tribution of interseismic processes that may differ from the subsequent interseismic period. If the possibility that fault coupling (Mavromatis et al., 2014) and/or tectonic plate motion (Heiki and Mitsui, 2013) has changed is not considered in analysis of postseismic geodetic data, inference of, for example, the rheological structure of the lower crust and upper mantle may be incorrect. The occurrence of afterslip itself defines a temporary change in the distribution of coupling and may persist for the duration of the epochs analyzed here. This afterslip may have longer-lived and/or farther-reaching effects by changing the pattern of resumed coupling across the earthquake source. Even under our assumption that the contribution to station motion from coupling is as temporally stable as possible, the Tokachi-oki and Tohoku-oki earthquakes perturb the distributions of strong coupling and thrust-sense slip. For example, a southwestward-migrating patch of deep thrust slip during Epochs 3 and 4 beneath the Hokkaido coastline (Fig. 7c, d) locally reduces the down-dip extent of strong coupling (Fig. 6c, d).

Covariance between signatures of resumed coupling and postseismic deformation (Figs. 2, 3) demonstrates the ambiguity in uniquely ascribing observed deformation to particular underlying physical processes. Sun et al. (2014) note that the assumed thickness of the subducting slab and viscosity of the mantle wedge between the subducting and overriding plates influence the temporal evolution of postseismic displacement in a manner similar to our assumed exponential decay times. In fitting geodetic time series, we attribute the linear component within each epoch to represent time-averaged tectonic and fault coupling processes, but we do not attribute the exponentially decaying motion to physical parameters. Nonetheless, covariance between contributions from interpreted fault coupling and postseismic deformation indicates that interpretation of rheological parameters from the postseismic form would be non-unique without independent constraints on the spatiotemporal distribution of coupling.

#### 4.2. Effect of exponential decay constant on coupling estimate

The results described above make the inherent assumption that the spatial distribution of subduction zone coupling has varied as little as possible since Epoch 1, yet we do in fact see notable changes. If, rather than assuming spatially and temporally variable postseismic duration in estimating nominally interseismic velocity fields used to constrain block models, we assume a single exponential decay constant since 1996, we estimate differences in coupling patterns relative to MVVF results in Epochs 3–5 following the 2003 Tokachi-oki earthquake. Assuming a 3-year

decay duration (Fig. 8a) shows a region of strong coupling offshore Hokkaido during Epoch 3 that is narrower down-dip than the corresponding MVVF patch (Fig. 6c), representing postseismic deformation convolved with interseismic coupling, and generally similar patterns of coupling off Tohoku and on the Sagami and Nankai interfaces. Coupling during Epoch 4 (Fig. 8a) shows reduced southwest extent of the Tohoku patch similar to the MVVF model (Fig. 6d). Coupling offshore Hokkaido is less than half the area of the MVVF model, separated from a distinct coupling patch at 41°N. On the Nankai Trough, the southern coupling patch extends farther southwest than the MVVF patch. For Epoch 5, the 3-year decay velocity field yields a region of strong coupling from 40°N to the northeast extent of the modeled interface offshore Hokkaido (Fig. 8a), nearly identical in extent to the Epoch 4 coupling in the MVVF model (Fig. 6d). Around Tohoku, we estimate coupling entirely  $<80\%$ , consistent with nominally interseismic velocities that in fact contain substantial postseismic deformation owing to the short assumed decay duration, which has been attributed by several studies to afterslip (Diao et al., 2013; Evans and Meade, 2012; Ozawa et al., 2012; Yamagiwa et al., 2015). Epoch 5 coupling also differs substantially in the 3-year decay model compared to the MVVF model (Fig. 6e) on the Nankai Trough, with more spatially contiguous coupling spanning nearly the entire modeled interface.

Assuming a 5-year decay duration (Fig. 8b) results in strong Epoch 3 coupling that is similar to that of the MVVF model, though coupling on the southern Japan Trench and Nankai Trough is more spatially contiguous. During Epoch 4, coupling is more segmented than the MVVF offshore Hokkaido and about 65% more extensive offshore Tohoku. Coupling is similar to the MVVF model on the Nankai interface except near the southwest extent of the southern patch. Epoch 5 shows similarities in coupling with the 3-year decay model, with contiguous coupling across the Nankai Trough, no strong coupling in the Tohoku-oki region, and coupling north of 40° that is 70% larger than that of the MVVF model, similar to the MVVF Epoch 4 distribution.

Using a 7-year decay time (Fig. 8c) yields strong coupling during Epoch 3 similar to the MVVF offshore Hokkaido and central Tohoku, but a patch is also estimated on the deep part of the southern Japan Trench, as in the 5-year decay model. Coupling is continuous across the entire Nankai interface. During Epoch 4, coupling in the 7-year model is similar offshore Hokkaido and on the Sagami and Nankai Troughs, and double in area off Tohoku compared to the MVVF model. In Epoch 5, the 7-year decay model is segmented offshore Hokkaido and around the bend of the Japan-Kuril Trench, unlike in the MVVF model (Fig. 6e), and there is again

little coupling in the Tohoku-oki region, consistent with the MVVF-estimated postseismic durations  $\geq 7$  years along the Tohoku coast.

#### 4.3. Coupling, aseismic slip, and seismic hazard implications

The distribution of interseismic coupling imaged before the 2005 Nias (Sumatra), 2007 Mentawai (Sumatra), 2011 Tohoku-oki, 2012 Nicoya (Costa Rica), and 2014 Iquique (Chile) subduction zone earthquakes shows positive spatial correlation with the pattern of coseismic slip (Konca et al., 2008; Li et al., 2015; Loveless and Meade, 2011; Protti et al., 2014). For the Tohoku-oki earthquake, a region coupled  $\geq 30\%$  of the long-term convergence rate, estimated from the Epoch 1 velocity field, shows strong spatial correlation with the region that slipped coseismically  $\geq 4$  m (Loveless and Meade, 2011). Examining the temporal evolution of strong coupling offshore central Tohoku (Fig. 6), we see consistency in the location and more than doubling in area of the  $\geq 80\%$  coupled patch from Epoch 1 to Epoch 2, and substantial expansion downdip and north along strike in Epoch 3, with total patch area more than 3 times that of Epoch 1. In Epoch 4, preceding the 2011 Tohoku-oki earthquake, the coupled region remains constant in area but shows a northward shift. Concurrently, we estimate thrust-sense slip (Fig. 7d) at this downdip extent. This zone of forward-sense slip near the southern extent of the Tohoku-oki rupture zone is consistent with the suggestion of Mavrommatis et al. (2014), who modeled GEONET position time series considering an acceleration term in addition to velocity and interpreted a decadal-scale aseismic transient in the region of our estimated thrust slip during Epoch 4.

The Sanriku-oki region offshore northern Tohoku ( $39^\circ$ – $40^\circ$ N) experienced a  $M_W = 7.7$  earthquake in 1994 with a period of afterslip lasting about 5 years (Heki et al., 1997; Nishimura et al., 2004). The southward expansion of the off-Hokkaido coupled patch and northward expansion of the off-Tohoku patch (in TC models) during Epochs 2–4 are consistent with resumed coupling in this region at depths of 20–40 km since the beginning of Epoch 2. At depths  $\geq 60$  km beneath the northern Tohoku coast, we image thrust slip in all epochs, though the area and centroid of this thrust-slipping region vary through time, such that, except for 4 triangular dislocation elements, no given portion of the interface slips in all epochs (Fig. 7f). The combination of deep, thrust-sense slip and gradual resumption of coupling in the Sanriku-oki region since 1994 may have limited the northern rupture extent of the 2011 Tohoku-oki earthquake, serving as a kinematic barrier to rupture that had not accumulated sufficient moment to allow that event to propagate north of  $\sim 38^\circ$ N (Loveless and Meade, 2015).

The northern concentration of strong coupling on the Japan-Kuril Trench subduction zone, offshore Hokkaido, is consistently larger in area than that coinciding with the  $M_W = 9.0$  Tohoku-oki earthquake, particularly during Epochs 2–4. Great earthquakes offshore Hokkaido have historically been substantially smaller than the Tohoku-oki event – the 1952 and 2003 Tokachi-oki earthquakes were both  $M_w \sim 8.2$  – but there is precedent for  $M_w \sim 9$ -class earthquakes rupturing the interface beneath the entire Hokkaido coastline with a  $\sim 500$ -year recurrence interval (Nanayama et al., 2003). Such events are more consistent with the total area of  $\geq 80\%$  coupling in this region (Loveless and Meade, 2015), even given temporal variation in the distribution of coupling and thrust-sense slip before and after the 2003 Tokachi-oki event (Figs. 6, 7).

Strong coupling on the western Sagami Trough, beneath the Boso Peninsula and Tokyo Bay, has varied in area through time but remains consistent in location (Fig. 6). Episodic, aseismic slow slip events (SSEs) in May 1996, October 2002, and August 2007 on the eastern portion of the Sagami interface (Ozawa et al., 2003; Ozawa et al., 2007) may serve to modulate the nature of earth-

quakes across the entire subduction zone, temporarily reducing the total area of strong coupling, which may thereby reduce overall long-term seismic hazard. Our  $\sim 3.75$ -year epoch analysis does not resolve these 1–2 week duration SSEs, in that the characteristic reversal in velocity direction is not imaged, but estimated Epoch 2 velocities on the Boso Peninsula are reduced in magnitude and directed more southeasterly relative to Epoch 1 (Fig. 5a). The 1996 and 2007 SSEs occur near the beginnings of Epochs 1 and 4, respectively, and the reversal in east and north position is captured primarily by the ordinate-intercept term at epoch initiation. On the other hand, the 2002 event occurs about three-quarters of the Epoch 2 duration, and so it has greater impact than the other SSEs in reducing estimated northwest-directed velocity relative to adjacent epochs. If strain accumulation due to coupling on the eastern portion is partially relieved by periodic SSEs, the recurrence of large, 1703 Genroku-type earthquakes rupturing much of the Sagami interface could be delayed, and between these larger events, a greater number of 1923 Kanto earthquake-type events take place on the western part of the interface.

On the Nankai subduction interface, we image spatiotemporal stability in coupling since 1996. Strongly coupled patches offshore Shikoku and offshore the Kii Peninsula are present in each epoch, with spatiotemporal fluctuation limited primarily to the southwest extent of the southern patch near the Bungo Channel and the Tokai area, both known localities of episodic SSEs (Miyazaki et al., 2006; Ozawa et al., 2013). Bungo Channel SSEs in 1997, 2003, and 2010 have been interpreted from time series analysis of local GEONET stations (Ozawa et al., 2013). The 2003 event occurred near the transition from Epoch 2 to 3, and the lack of reduced coupling area we estimate during those epochs may suggest that velocity change due to the SSE may have been absorbed into the postseismic signal estimated for the Tokachi-oki earthquake. However, the 1997 and 2010 events occurred during Epochs 1 and 4, respectively, when the southwest extent of the southern strong coupling patch was reduced (Fig. 6a, d). Importantly, even if the SSE duration is shorter than our  $\sim 3.75$ -year epochs, it may serve to reduce the effective coupling below 80% during the epoch in which it occurs.

The coupled regions are spatially consistent with the estimated rupture areas of Nankai/Tonankai and Tokai type earthquakes, respectively (Furumura et al., 2011; Kodaira et al., 2006). Our persistent strong coupling region extends farther southwest than several rupture models for the 1946 earthquake (Sagiya and Thatcher, 1999; Tanioka and Satake, 2001) but is consistent with recent rupture scenarios for the 1707, whole-margin Hoei-type earthquake based on tsunami records (Hyodo et al., 2014). The separation between the Shikoku and Kii patches is spatially coincident with a subducted seamount that has been seismically imaged and proposed as a potential barrier to megathrust ruptures, including during the 1946 great Nankaido earthquake (Kodaira et al., 2006). The temporal persistence of these segmented coupling zones is conceptually consistent with long-term geologic control on earthquake cycle behavior by this subducted seamount.

While physical properties of the subduction interfaces may exert influence on seismogenic behavior, it is unclear which properties could vary on sub-decadal time scales. We suggest that fluctuations in fluid pressure on the interface may be induced by large coseismic stress changes such as those induced by the Tokachi-oki and Tohoku-oki earthquakes and could explain some spatiotemporal variations in coupling. In particular, the dramatic contraction in area of the coupled patch offshore Hokkaido following the Tohoku-oki earthquake may suggest that interface fluid pressure increased as a result of coseismic stressing.

## 5. Conclusions

We analyzed GEONET position time series from 1996–2014 in five, ~3.75-year epochs in order to assess the spatiotemporal evolution of interseismic coupling on the Japanese subduction zones. Estimated transient postseismic deformation following major earthquakes covaries with interseismic deformation, such that a change in the spatial distribution of subduction zone coupling could be interpreted as an off-fault postseismic effect such as viscoelastic relaxation. To address this covariance, we describe the duration of postseismic deformation uniquely for each station and each epoch, assuming that the interseismic contribution to station motion is as consistent as possible through time. Even under this assumption that interseismic deformation patterns are temporally stable, subduction zone coupling shows a remarkable diversity of behavior through time, including:

- A large region of strong coupling offshore Hokkaido that was reduced in area by the 2003 Tokachi-oki earthquake and postseismic deformation as well as by the more distal 2011 Tohoku-oki earthquake, but is consistent in spatial extent with infrequent  $M_w \sim 9$ -class earthquakes inferred from the paleoseismic record (Nanayama et al., 2003);
- Resumed coupling in the Sanriku-oki region following the 1994 earthquake, as shown by expansion of coupled patches offshore Tohoku (northward) and Hokkaido (southward);
- Reduction in southern extent of strong coupling offshore Tohoku that is consistent with deep, aseismic thrust-sense slip preceding the 2011 Tohoku-oki earthquake (Mavrommatis et al., 2014);
- Stability of strong coupling on the Sagami Trough interface, restricted to a region west of the Boso Peninsula;
- Stability of coupling across much of the Nankai Trough, with the exception of around Tokai, which has experienced several slow slip events, including a long-duration event from 2000–2005 (Miyazaki et al., 2006), and the southwest extent of the coupled patch offshore Shikoku around the Bungo Channel, which has also featured episodic slow slip (Ozawa et al., 2013). Persistent strong coupling corresponds to regions interpreted to have slipped in historical great earthquakes.

These time-dependent images of decadal variations in subduction zone coupling reveal a diversity of behaviors from invariance to variability, challenge the notion of universally persistent seismic asperities, and are consistent with the idea that continued long-period geodetic observations may further expand the known range of earthquake cycle behaviors.

## Acknowledgements

We gratefully acknowledge the Geospatial Information Authority of Japan (GSI) for providing access to GEONET data. Information on seismicity comes from the Global CMT Project. We thank Hannah Baranes, Michele Cooke, Louisa Hall, and Jon Woodruff for helpful discussion, and two anonymous referees for thorough, thoughtful reviews. Most figures were generated using the Generic Mapping Tools (Wessel et al., 2013). The elastic block modeling code is available at <https://github.com/brendanjmeade/Blocks>. Loveless was supported by a Jean Picker Fellowship from Smith College.

## Appendix A. Supplementary material

Supplementary material related to this article can be found online at <http://dx.doi.org/10.1016/j.epsl.2015.12.033>.

## References

- Apel, E.V., Burgmann, R., Steblov, G., Vasilenko, N., King, R., Prytkov, A., 2006. Independent active microplate tectonics of northeast Asia from GPS velocities and block modeling. *Geophys. Res. Lett.* 33, L11303. <http://dx.doi.org/10.1029/2006GL026077>.
- Bird, P., 2003. An updated digital model of plate boundaries. *Geochem. Geophys. Geosyst.* 4, 1027. <http://dx.doi.org/10.1029/2001GC000252>.
- Diao, F., Xiong, X., Wang, R., Zheng, Y., Walter, T.R., Weng, H., Li, J., 2013. Overlapping post-seismic deformation processes: afterslip and viscoelastic relaxation following the 2011  $M_w 9.0$  Tohoku (Japan) earthquake. *Geophys. J. Int.* 196, 218–229. <http://dx.doi.org/10.1093/gji/ggt376>.
- Dragert, H., Wang, K., James, T.S., 2001. A silent slip event on the deeper Cascadia subduction interface. *Science* 292, 1525–1528. <http://dx.doi.org/10.1126/science.1060152>.
- Ergintav, S., McClusky, S., Hearn, E., Reilinger, R., Cakmak, R., Herring, T., Ozener, H., Lenk, O., Tari, E., 2009. Seven years of postseismic deformation following the 1999,  $M = 7.4$  and  $M = 7.2$  Izmit-Düzce, Turkey earthquake sequence. *J. Geophys. Res.* 114. <http://dx.doi.org/10.1029/2008JB006021>.
- Evans, E.L., Meade, B.J., 2012. Geodetic imaging of coseismic slip and postseismic afterslip: sparsity-promoting methods applied to the great Tohoku earthquake. *Geophys. Res. Lett.* 39, L11314. <http://dx.doi.org/10.1029/2012gl051990>.
- Furumura, T., Imai, K., Maeda, T., 2011. A revised tsunami source model for the 1707 Hoei earthquake and simulation of tsunami inundation of Ryujin Lake, Kyushu, Japan. *J. Geophys. Res.* 116, B02308. <http://dx.doi.org/10.1029/2010JB007918>.
- Furuse, N., Kono, Y., 2003. Slab residual gravity anomaly: gravity reduction due to subducting plates beneath the Japanese Islands. *J. Geodyn.* 36, 497–514. [http://dx.doi.org/10.1016/S0264-3707\(03\)00062-0](http://dx.doi.org/10.1016/S0264-3707(03)00062-0).
- Gagnon, K., Chadwell, C.D., Norabuena, E., 2005. Measuring the onset of locking in the Peru-Chile trench with GPS and acoustic measurements. *Nature* 434, 205–208. <http://dx.doi.org/10.1038/nature03412>.
- Hashimoto, C., Noda, A., Sagiya, T., Matsu'ura, M., 2009. Interplate seismogenic zones along the Kuril-Japan trench inferred from GPS data inversion. *Nat. Geosci.* 2, 141–144. <http://dx.doi.org/10.1038/ngeo421>.
- Hashimoto, M., Jackson, D.D., 1993. Plate tectonics and crustal deformation around the Japanese islands. *J. Geophys. Res.* 98, 16149–16166. <http://dx.doi.org/10.1029/93JB00444>.
- Hashimoto, M., Miyazaki, S., Jackson, D.D., 2000. A block-fault model for deformation of the Japanese Islands derived from continuous GPS observation. *Earth Planets Space* 52, 1095–1100. <http://dx.doi.org/10.1186/BF03352337>.
- Hearn, E.H., McClusky, S., Ergintav, S., Reilinger, R.E., 2009. Izmit earthquake postseismic deformation and dynamics of the North Anatolian Fault Zone. *J. Geophys. Res.* 114, B08405. <http://dx.doi.org/10.1029/2008JB006026>.
- Heki, K., Mitsui, Y., 2013. Accelerated pacific plate subduction following interplate thrust earthquakes at the Japan trench. *Earth Planet. Sci. Lett.* 363, 44–49. <http://dx.doi.org/10.1016/j.epsl.2012.12.031>.
- Heki, K., Miyazaki, S., Tsuji, H., 1997. Silent fault slip following an interplate thrust earthquake at the Japan Trench. *Nature* 386, 595–597. <http://dx.doi.org/10.1038/386595a0>.
- Hirose, F., Nakajima, J., Hasegawa, A., 2008. Three-dimensional seismic velocity structure and configuration of the Philippine Sea slab in southwestern Japan estimated by double-difference tomography. *J. Geophys. Res.* 113, B09315. <http://dx.doi.org/10.1029/2007JB005274>.
- Hirose, H., Hirahara, K., Kimata, F., Fujii, N., Miyazaki, S.I., 1999. A slow thrust slip event following the two 1996 Hyuganada earthquakes beneath the Bungo Channel, southwest Japan. *Geophys. Res. Lett.* 26, 3237–3240. <http://dx.doi.org/10.1029/1999GL010999>.
- Hyodo, M., Hori, T., Ando, K., Baba, T., 2014. The possibility of deeper or shallower extent of the source area of Nankai Trough earthquakes based on the 1707 Hoei tsunami heights along the Pacific and Seto Inland Sea coasts, southwest Japan. *Earth Planets Space* 66, 1–14. <http://dx.doi.org/10.1186/1880-5981-66-123>.
- Ide, S., Baltay, A., Beroza, G.C., 2011. Shallow dynamic overshoot and energetic deep rupture in the 2011  $M_w 9.0$  Tohoku-Oki earthquake. *Science* 332, 1426–1429. <http://dx.doi.org/10.1126/science.1207020>.
- Ikuta, R., Satomura, M., Fujita, A., Shimada, S., Ando, M., 2012. A small persistent locked area associated with the 2011  $M_w 9.0$  Tohoku-Oki earthquake, deduced from GPS data. *J. Geophys. Res.* 117, B11408. <http://dx.doi.org/10.1029/2012JB009335>.
- Kodaira, S., Hori, T., Ito, A., Miura, S., Fujie, G., Park, J.-O., Baba, T., Sakaguchi, H., Kaneda, Y., 2006. A cause of rupture segmentation and synchronization in the Nankai trough revealed by seismic imaging and numerical simulation. *J. Geophys. Res.* 111, B09301. <http://dx.doi.org/10.1029/2005JB004030>.
- Konca, A.O., Avouac, J.-P., Sladen, A., Meltzner, A.J., Sieh, K., Fang, P., Li, Z., Galetzka, J., Genrich, J., Chlieh, M., Natawidjaja, D.H., Bock, Y., Fielding, E.J., Ji, C., Helmberger, D.V., 2008. Partial rupture of a locked patch of the Sumatra megathrust during the 2007 earthquake sequence. *Nature* 456, 631–635. <http://dx.doi.org/10.1038/nature07572>.
- Li, S., Moreno, M., Bedford, J., Rosenau, M., Oncjen, O., 2015. Revisiting viscoelastic effects on interseismic deformation and locking degree: a case study of the Peru–North Chile subduction zone. *J. Geophys. Res.* 120, 4522–4538. <http://dx.doi.org/10.1002/2015JB011903>.

- Liu, Z., Owen, S., Dong, D., Lundgren, P., Webb, F., Hetland, E., Simons, M., 2010. Estimation of interplate coupling in the Nankai trough, Japan using GPS data from 1996 to 2006. *Geophys. J. Int.* 181, 1313–1328. <http://dx.doi.org/10.1111/j.1365-246X.2010.04600.x>.
- Loveless, J.P., Meade, B.J., 2010. Geodetic imaging of plate motions, slip rates, and partitioning of deformation in Japan. *J. Geophys. Res.* 115, B02410. <http://dx.doi.org/10.1029/2008JB006248>.
- Loveless, J.P., Meade, B.J., 2011. Spatial correlation of interseismic coupling and coseismic rupture extent of the 2011  $M_w = 9.0$  Tohoku-oki earthquake. *Geophys. Res. Lett.* 38, L17306. <http://dx.doi.org/10.1029/2011GL048561>.
- Loveless, J.P., Meade, B.J., 2015. Kinematic barrier constraints on the magnitudes of additional great earthquakes off the East Coast of Japan. *Seismol. Res. Lett.* 86, 202–209. <http://dx.doi.org/10.1785/0220140083>.
- Mavrommatis, A.P., Segall, P., Johnson, K.M., 2014. A decadal-scale deformation transient prior to the 2011  $M_w 9.0$  Tohoku-oki earthquake. *Geophys. Res. Lett.* 41, 4486–4494. <http://dx.doi.org/10.1002/2014GL060139>.
- McCaffrey, R., Long, M., Goldfinger, C., Zwick, P.C., Nabalek, J.L., Johnson, C.K., Smith, C., 2000. Rotation and plate locking at the southern Cascadia subduction zone. *Geophys. Res. Lett.* 27, 3117–3120. <http://dx.doi.org/10.1029/2000GL011768>.
- Meade, B.J., Loveless, J.P., 2009. Block modeling with connected fault network geometries and a linear elastic coupling estimator in spherical coordinates. *Bull. Seismol. Soc. Am.* 99, 3124–3139. <http://dx.doi.org/10.1785/0120090088>.
- Miyazaki, S.i., Segall, P., McGuire, J.J., Kato, T., Hatanaka, Y., 2006. Spatial and temporal evolution of stress and slip rate during the 2000 Tokai slow earthquake. *J. Geophys. Res.* 111, B03409. <http://dx.doi.org/10.1029/2004JB003426>.
- Mogi, K., 1958. Relations between the eruptions of various volcanoes and the deformations of the ground surface around them. *Bull. Earthq. Res. Inst. Univ. Tokyo* 36, 99–134.
- Nakamura, M., 2004. Crustal deformation in the central and southern Ryukyu Arc estimated from GPS data. *Earth Planet. Sci. Lett.* 217, 389–398. [http://dx.doi.org/10.1016/S0012-821X\(03\)00604-6](http://dx.doi.org/10.1016/S0012-821X(03)00604-6).
- Nakata, T., Imaizumi, T., 2002. Digital Active Fault Map of Japan. University of Tokyo Press, Tokyo.
- Nanayama, F., Satake, K., Furukawa, R., Shimokawa, K., Atwater, B.F., Shigeno, K., Yamaki, S., 2003. Unusually large earthquakes inferred from tsunami deposits along the Kuril trench. *Nature* 424, 660–663. <http://dx.doi.org/10.1038/Nature01864>.
- Nishimura, S., Hashimoto, M., 2006. A model with rigid rotations and slip deficits for the GPS-derived velocity field in Southwest Japan. *Tectonophysics* 421, 187–207. <http://dx.doi.org/10.1016/j.tecto.2006.04.017>.
- Nishimura, T., Hirasawa, T., Miyazaki, S., Sagiya, T., Tada, T., Miura, S., Tanaka, K., 2004. Temporal change of interplate coupling in northeastern Japan during 1995–2002 estimated from continuous GPS observations. *Geophys. J. Int.* 157, 901–916. <http://dx.doi.org/10.1111/j.1365-246X.2004.02159.x>.
- Nishimura, T., Sagiya, T., Stein, R.S., 2007. Crustal block kinematics and seismic potential of the northernmost Philippine Sea plate and Izu microplate, central Japan, inferred from GPS and leveling data. *J. Geophys. Res.* 112, B05414. <http://dx.doi.org/10.1029/2005JB004102>.
- Ochi, T., Kato, T., 2013. Depth extent of the long-term slow slip event in the Tokai district, central Japan: a new insight. *J. Geophys. Res.* 118, 4847–4860. <http://dx.doi.org/10.1002/jgrb.50355>.
- Ozawa, S., Miyazaki, S., Hatanaka, Y., Imakiire, T., Kaidzu, M., Murakami, M., 2003. Characteristic silent earthquakes in the eastern part of the Boso peninsula, Central Japan. *Geophys. Res. Lett.* 30, 1283. <http://dx.doi.org/10.1029/2002GL016665>.
- Ozawa, S., Nishimura, T., Munekane, H., Suito, H., Kobayashi, T., Tobita, M., Imakiire, T., 2012. Preceding, coseismic, and postseismic slips of the 2011 Tohoku earthquake, Japan. *J. Geophys. Res.* 117, B07404. <http://dx.doi.org/10.1029/2011JB009120>.
- Ozawa, S., Suito, H., Tobita, M., 2007. Occurrence of quasi-periodic slow-slip off the east coast of the Boso peninsula, Central Japan. *Earth Planets Space* 59, 1241–1245. <http://dx.doi.org/10.1186/BF03352072>.
- Ozawa, S., Yara, H., Imakiire, T., Tobita, M., 2013. Spatial and temporal evolution of the long-term slow slip in the Bungo Channel, Japan. *Earth Planets Space* 65, 67–73. <http://dx.doi.org/10.5047/eps.2012.06.009>.
- Pollitz, F.F., Peltzer, G., Bürgmann, R., 2000. Mobility of continental mantle: evidence from postseismic geodetic observations following the 1992 Landers earthquake. *J. Geophys. Res.* 105, 8035–8054. <http://dx.doi.org/10.1029/1999JB900380>.
- Protti, M., Gonzalez, V., Newman, A.V., Dixon, T.H., Schwartz, S.Y., Marshall, J.S., Feng, L., Walter, J.I., Malservisi, R., Owen, S.E., 2014. Nicoya earthquake rupture anticipated by geodetic measurement of the locked plate interface. *Nat. Geosci.* 7, 117–121. <http://dx.doi.org/10.1038/ngeo2038>.
- Sagiya, T., Miyazaki, S., Tada, T., 2000. Continuous GPS array and present-day crustal deformation of Japan. *Pure Appl. Geophys.* 157, 2303–2322. <http://dx.doi.org/10.1007/PL00022507>.
- Sagiya, T., Thatcher, W., 1999. Coseismic slip resolution along a plate boundary megathrust: the Nankai Trough, southwest Japan. *J. Geophys. Res.* 104, 1111–1129. <http://dx.doi.org/10.1029/98JB02644>.
- Sun, T., Wang, K., Iinuma, T., Hino, R., He, J., Fujimoto, H., Kido, M., Osada, Y., Miura, S., Ohta, Y., Hu, Y., 2014. Prevalence of viscoelastic relaxation after the 2011 Tohoku-oki earthquake. *Nature* 514, 84–87. <http://dx.doi.org/10.1038/nature13778>.
- Tanioka, Y., Satake, K., 2001. Coseismic slip distribution of the 1946 Nankai earthquake and aseismic slips caused by the earthquake. *Earth Planets Space* 53, 235–241. <http://dx.doi.org/10.1186/BF03352380>.
- Toda, S., Stein, R.S., Kirby, S.H., Bozkurt, S.B., 2008. A slab fragment wedged under Tokyo and its tectonic and seismic implications. *Nat. Geosci.* 1, 771–776. <http://dx.doi.org/10.1038/ngeo318>.
- Wessel, P., Smith, W.H.F., Scharroo, R., Luis, J., Wobbe, F., 2013. Generic mapping tools: improved version released. *Eos* 94, 409–410. <http://dx.doi.org/10.1002/2013EO450001>.
- Yamagawa, S., Miyazaki, S.i., Hirahara, K., Fukahata, Y., 2015. Afterslip and viscoelastic relaxation following the 2011 Tohoku-oki earthquake ( $M_w 9.0$ ) inferred from inland GPS and seafloor GPS/Acoustic data. *Geophys. Res. Lett.* 42, 66–73. <http://dx.doi.org/10.1002/2014GL061735>.